Biomedical Microdevices (2020) 22:20
https://doi.org/10.1007/s10544-020-0474-x

# Cell trapping microfluidic chip made of Cyclo olefin polymer enabling two concurrent cell biology experiments with long term durability

Elif Gencturk[1] · Ekin Yurdakul[1] · Ahmet Yasin Celik[2] · Senol Mutlu[2] · Kutlu O. Ulgen[1]



**Abstract**
Cyclo Olefin Polymer (COP) based microbioreactors on a microfluidic chip were produced in house by hot-embossing and thermo-compression bonding methods. The chip allows two different experiments to be performed on trapped cells at the same time. On one side of the chip, red fluorescent protein (RFP) tagged nucleolar Nop56 protein was used to track changes in cell cycle as well as protein synthesis within the yeast cells under the application of the anti-tumor agent hydroxyurea (HU). Simultaneously, on the other side of the chip, the response of yeast cells to the drug metformin, mTOR inhibitor, was investigated to reveal the role of TOR signaling in ribosome biogenesis and cell proliferation. The results of 20 h long experiments are captured by taking brightfield and fluorescent microscopy images of the trapped cells every 9 min. The expression of Nop56 protein of ribosome assembly and synthesis was densely observed during G1 phase of cell cycle, and later towards the end of cell cycle the ribosomal protein expression slowed down. Under HU treatment, the morphology of yeast cells changed, but after cessation of HU, the biomass synthesis rate was sustained as monitored by the cell perimeter. Under metformin treatment, the perimeters of single cells were observed to decrease, implying a decrease in biomass growth; however these cells continued their proliferation during and after the drug application. The relation between ribosome biogenesis and cell cycle was successfully investigated on single cell basis, capturing cell-to-cell variations, which cannot be tracked by regular macroscale bioreactors.

**Keywords** Nop56 · Ribosome biogenesis · Anti-tumor agent · Microbioreactor · COP

## 1 Introduction

Microfluidic platforms have become popular for experimental cell studies in recent years since they enable less material/volume consumption, fast result acquisition and single cell tracking. In conventional bioreactor experiments, average properties of cell populations inside a specific volume are measured, while in microfluidic devices the same cell can be monitored from the beginning to the end of the experiment under continuous flow. Performing single cell study in a microfluidic system is a robust and sensitive method to track cell-to-cell variations. Being a closed system and maintaining a controlled environment, risk of contamination is minimized in microfluidic bioreactors. Real-time monitoring of cells in response to input feeding is possible. Cell division, volume change and fluorescently tagged specific protein expression can be monitored on single cell basis.

The perturbations like drug or inhibitor applications to microbial cells often prolong the cell cycle and experiment time. Thus, when working with these cells, the materials used to fabricate microfluidic devices (microbioreactors) must be durable. One of the well-known and mostly used material for microfluidic studies is polydimethylsiloxane (PDMS). PDMS is biocompatible, transparent and it has low autofluorescence (Bélanger and Marois 2001; Piruska et al. 2005). However, absorption of hydrophobic molecules by PDMS is one of the main drawback of this material. Working with drug solutions or biomolecules for extended hours is difficult in PDMS devices (Toepke and Beebe 2006). Surface treatment of PDMS is also necessary to eliminate its hydrophobicity (Trantidou et al. 2017). Due to the

**Electronic supplementary material** The online version of this article (https://doi.org/10.1007/s10544-020-0474-x) contains supplementary material, which is available to authorized users.

✉ Kutlu O. Ulgen
ulgenk@boun.edu.tr

[1] Department of Chemical Engineering, Biosystems Engineering Laboratory, Bogazici University, 34342 Istanbul, Turkey

[2] Department of Electrical and Electronics Engineering, BUMEMS Laboratory, Bogazici University, 34342 Istanbul, Turkey

Published online: 20 February 2020

mentioned disadvantages of PDMS, thermoplastic made microfluidic chips have been developed as alternatives (Gencturk et al. 2017). Thermoplastic materials can be softened via heat and pressure and they harden after cooling, taking the shape of the desired device without going through any chemical modification (Odabasi et al. 2018). Among several thermoplastics, cyclo-olefin polymer (COP) is selected as the material for the fabrication of the microbioreactors because it is biocompatible for biological studies and transparent for visualization. It has low auto-fluorescence and high dimensional stability. Moreover, COP is suitable for mass manufacturing process and it is durable for long-hours of cell culture experiments (Puza et al. 2017).

*Saccharomyces cerevisiae* (*S. cerevisiae*) is a widely used eukaryotic model organism in molecular and cell biology studies due to its complex genetic structure, rapid growth ability in optimum conditions and easy replication properties (Sherman 1997). Ease of manipulation and genetic tractability make yeast cells more attractive for mammalian cell protein analysis. 31% of proteins encoded by yeast genes have human homologs and vice versa. Therefore, yeast is a valuable predictor of human gene functions, and has increased the knowledge of the principal pathways in humans and has promoted the awareness of many disease genes (La Ferla et al. 2015), including ribosomopathies, the human disease that influences ribosome biogenesis (Woolford and Baserga 2013). In the literature, there are several works conducted with yeast cells in microfluidic platforms. High-throughput microfluidic imaging system for single yeast cell tracking was performed over multiple generations (Falconnet et al. 2011; Hansen et al. 2015). More recently, microfluidic devices were developed to investigate various biological issues like spatial variation in yeast cell growth in heterogeneous environment, the formation of gene expression landscapes (Marinkovic et al. 2019), protein dynamics during sporulation of yeast cells (Zhao et al. 2019), long term imaging of yeast cells under constant or changing environment, DNA damage using of genotoxic chemicals (Schmidt et al. 2018), and isolation of cells in an automated system (Yu et al. 2018). Microfluidic impedance cytometry was used to combine cell impedance with yeast cell morphology (Haandbæk et al. 2016). There are also review papers about yeast cells in microfluidic devices with several applications (Dusny and Grünberger 2020; Jo and Qin 2016).

In the present study, we designed a new microfluidic chip and fabricated it using COP substrates. With the new design, it is now possible to conduct two different experiments at the same time unlike the previous designs (Odabasi et al. 2018; Puza et al. 2017). Two different strains in one medium or two different media with single strain can be operated in this platform. Comsol 5.2 software with microfluidics module was used to determine the system dynamics of the designed device. Here, our focus is to show the benefit of our dual purpose design of new microfluidic chip in experimentation. We applied this improved design for observing the processes of cell cycle and ribosome synthesis in yeast on single cell basis (RFP-tagged Nop56 protein of *S. cerevisiae)*. The drugs, hydroxyurea (HU), inhibitor of DNA, and metformin, inhibitor of mTOR pathway, are employed for the first time in a microfluidic platform to reveal the relationship between the cell cycle and ribosome biogenesis. The ultimate aim is to examine the response of cells to these growth inhibitory drugs, as cancer therapy agents, deciphering the link between ribosome assembly (pre-processing) and cell cycle.

## 2 Experimental section

### 2.1 Materials

The strain used in this study is *Saccharomyces cerevisiae* (EY0987 genetic background Matα his3Δ1 leu2Δ0 lys2Δ0 ura3Δ0 (S288C)) with the RFP tagged YLR197W (Nop56p) gene, kindly provided by Peter Arvidson from Harvard University, HHMI. Cyclo olefin polymer (COP) (Product code: Zeonor 10–0672–0349-1.0-05) was purchased from Microfluidic ChipShop Company (Jena, Germany). Polyethylene tubing (Product code: BB31695-PE/6) and epoxy (5 min epoxy) are products of Scientific Commodities Inc. SCI (Lake Havasu City, AZ 86406, The USA) and BISON (Rotterdam, The Netherlands), respectively. All the chemicals and reagents (including HU) used for medium preparation were purchased from Sigma-Aldrich (Taufkirchen, Germany) and metformin was purchased from a local pharmacy under the brand name of Diaformin.

### 2.2 Design of the microfluidic device

The experimental setup is shown in Fig. 1. The new design used in this study was improved considering the shortcomings of the devices used in the previous studies (Odabasi et al. 2018; Puza et al. 2017). Working with single strain and single medium was one of the most cumbersome aspects of the previous design, consuming time and energy (workpower). The chambers are now placed in parallel fashion instead of series arrangement. This allowed the cells to be evenly distributed throughout each chamber and eliminated residues coming from the front chamber affect the rest of the chambers in series configuration. The present microfluidic device includes two different segments, each having 8 chambers with C-shaped regions, which are placed along the channels to trap the yeast cells (Fig. 1a). This design enables the cultivation of two different strains in one type of nutrient medium or the cultivation of one strain in two different nutrient media, i.e. there is no need for the exchange of cell culture and nutrient flows. The dedicated lines for yeast cells (b) and the nutrient medium (a & c) prevent any contamination among the channels (Fig. 1a). In

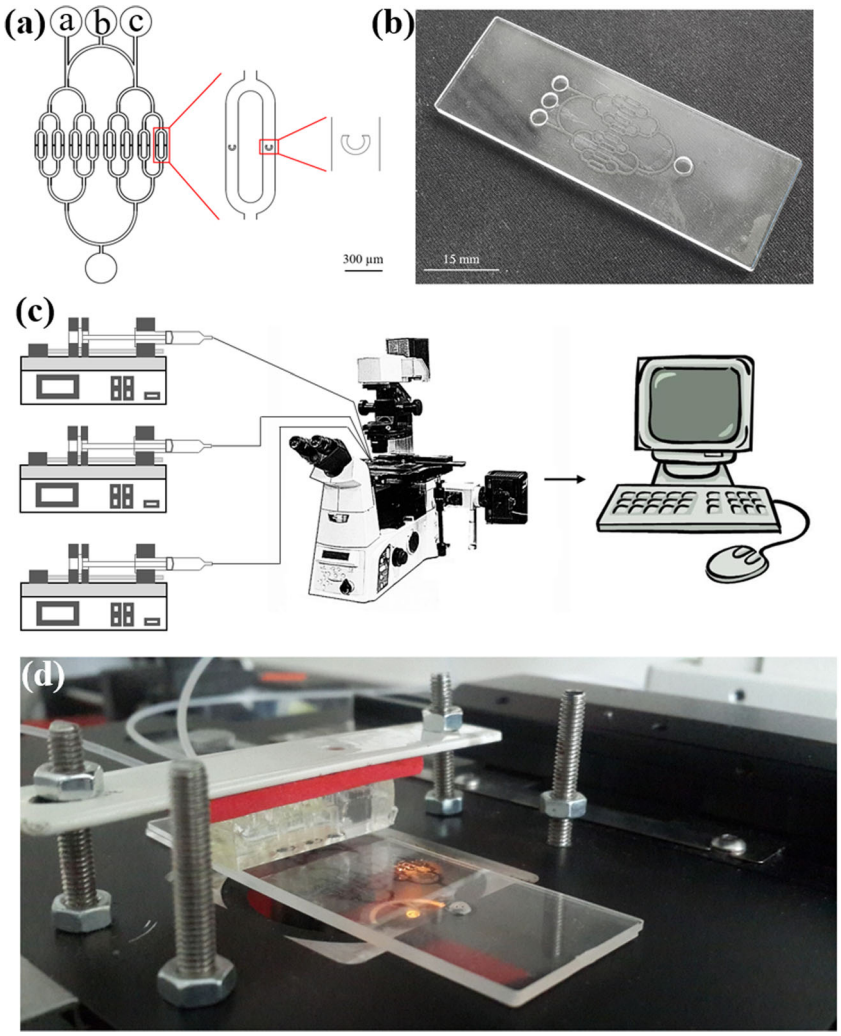


**Fig. 1** **a** Schematic illustration of the device design. **b** Fabricated microfluidic device. **c** Experimental setup. **d** In-house fabricated microbioreactor placed on microscopy stage with external tubing connections

addition, every chamber within the device act like an independent microbioreactor. Thus, two different experiments are repeated for 8 times.

## 2.3 Device fabrication

### 2.3.1 Drilling inlet-outlet reservoirs and planarization

Blank COP substrate of 75.5 mm × 25.5 mm × 1 mm (L x W x H) dimension is placed on the stage of computer numerical control (CNC) machine and the inlet and outlet holes are drilled automatically according to the coordinates of the design. The drilled COP piece is put into ultrasonic bath for 15 min and dried with $N_2$ gun. Burrs around inlets and outlet are cleaned via craft knife to have smooth surface for proper bonding. This COP sample is then pressed with the help of 2-mm-thick blank glass pieces using a hydraulic press machine. Glass pieces and COP are cleaned using baby shampoo, acetone, isopropyl alcohol (IPA) and distilled water, respectively. They are dried with $N_2$ gun. After this cleaning process, all of the pieces are stacked in the order of glass-COP-glass, covered with aluminum foil and placed on the hot plate of the hydraulic press machine, which was set to 130 °C. The system is warmed up for 10 min and then 35 bar pressure is applied for another 10 min. Finally the pieces are left for cooling to 60 °C for 1.5 h under pressure. The purpose of this pressing step is to remove any further bumps or burrs remaining on the surface after drilling.

### 2.3.2 Hot-embossing

Hot embossing process is conducted subsequently. For this step, a stainless steel mold had already been prepared using photolithography and electrochemical etching fabrication steps as explained in a previous work (Gokdel et al. 2010). This way micro patterns on steel surface were formed according to the design of the microfluidic device shown in Fig. 1a. This design was verified using a finite element analysis tool (COMSOL Multiphysics 5.2) before printing it on a physical mask for the lithography step. The stainless steel mold,

planarized COP substrate with inlet/outlet holes and a glass piece are cleaned as explained in the previous section. COP piece is placed on the mold, and the glass is put on its other side. A piece of aluminum foil is used to cover them. All are placed on the hot plates at 130 °C of the hydraulic press machine. The hot plates of the press machine are brought close to each other, and the pieces are let to reach the set temperature for 10 min. 35 bar pressure is applied for 10 min subsequent to the thermal stabilization. Finally, the pieces in the press machine are left to cool down to 60 °C under pressure for 1.5 h.

#### 2.3.3 Bonding

In this step, hot embossed COP piece and a blank COP piece are bonded together. Bonding process should be conducted below the glass transition temperature of the polymer to prevent the deterioration of the patterns on the hot embossed piece. The glass transition temperature of the COP is 136 °C and the temperature for bonding process is optimized as 125 °C. COP pieces are placed between glass ones and covered with a piece of aluminum foil. The cleaning procedure is carried out as described in previous sections. After pieces are thermally stabilized at the set temperature value, 25 bar pressure is applied for 45 min to start bonding. After this step, the temperature controller of the hydraulic press machine is set to room temperature to cool under pressure. Cooling process takes 3 h and glass pieces are separated from the bonded pieces carefully without damaging. Figure 1b shows the fabricated device.

### 2.4 Medium preparation and microscopy

Yeast nitrogen base (YNB) (2% glucose, yeast extract, nitrogen base) media were used during the experiments. Hydroxyurea (HU) was added dry to final concentration of 200 mM (prepared from powder form and not sterilized) and the optical density (OD) of the preculture loaded to the microfluidic device was 0.5 (600 nm). 1.25 g metformin in powder form was dissolved in 100 ml DMSO. 2 ml of metformin-DMSO solution was added to YNB medium and final concentration of metformin was 0.025%. Nikon Ti-E inverted fluorescence microscope with Nikon DS-Ri2 detector and Texas Red filter were used to detect Red Fluorescent Protein RFP:Nop56 tagged yeast cells. Brightfield and fluorescence microscopy images of the cells were taken during the experiments and ImageJ (NIH, Bethesta, MD) software was used to process the acquired images. Several filters and Otsu thresholding were applied to obtain cell count and perimeter values. Moreover, red channel was used to analyze fluorescence microscopy images of the cells in accordance with their RFP tagging. Figure 1c, d shows the experimental setup illustration and microbioreactor chip placed on the microscopy stage with established external tubing connnections, respectively.

### 2.5 Computational fluid dynamics (CFD) simulations

Various fluid dynamics simulations were performed to reach the optimum design for cell trapping. The main purpose of the simulation is to analyse design alternatives to achieve cell trapping in all C-shaped regions of 16 parallel microfluidic channels. In order to achieve this, two main modules (spf and fpt representing laminar flow and particle tracing for fluid flow, respectively) and a multi-physics module (fluid-particle interaction) were created and simulated in COMSOL 5.2. The design effort is based on creation of stagnation points in each channel inside the c shape. For this purpose, spf module was used to analyse the flow rates and directions in the channels. Fpt plays an important role to analyse particle movement under laminar flow condition that is solved by the multi-physics module. Mesh analysis is based on independent solver that allows us to observe same results on coarse, normal, fine and extra fine mesh designs (Fig. S1). Figure S2 shows velocity magnitude with stationary solution that helps to analyse the flow distribution in the microfluidic channel including inlet, outlet and no slip condition at wall. The simulation of trapping mechanism with parallel channel designs enables equal 16 stagnation points in C shaped regions. Due to the laminar flow, the stagnation point is observed inside the C shape and high velocity profile between the C shape and channel walls. Figure 2a shows velocity profile in the microfluidic channel with velocity field streamlines that also prove the stagnation point. After implementation of spf module of Comsol 5.2, fpt was implemented with the time dependent solver that enables to observe the trapping mechanism with different time scales. It can be clearly seen that every particle has unique speed because of its location, and particles follow the velocity profile of laminar flow. As the particle has higher velocity in the middle of the channel, it moves directly towards the stagnation point, other particles on the sides continue to move from the edge of the C shape to the outlet. Finally, several particles can be observed in the C shape in Fig. 2b.

### 2.6 Microfluidic device operation

First, the priming step of the microfluidic device with YNB medium was performed and then, yeast cells grown in the YNB medium were loaded into the device. Cells were trapped in the c-shaped regions of the chambers, and fresh YNB medium was sent through the device for 3–6 h. Thereafter, the drug administration (200 mM HU for one side of the chip and 0.025% metformin for the other side) was started, that lasted for another 3 h. Subsequently, fresh YNB medium was fed for the next 10 h for the recovery of cells until the end of the experiment. During these operations, the cells were monitored

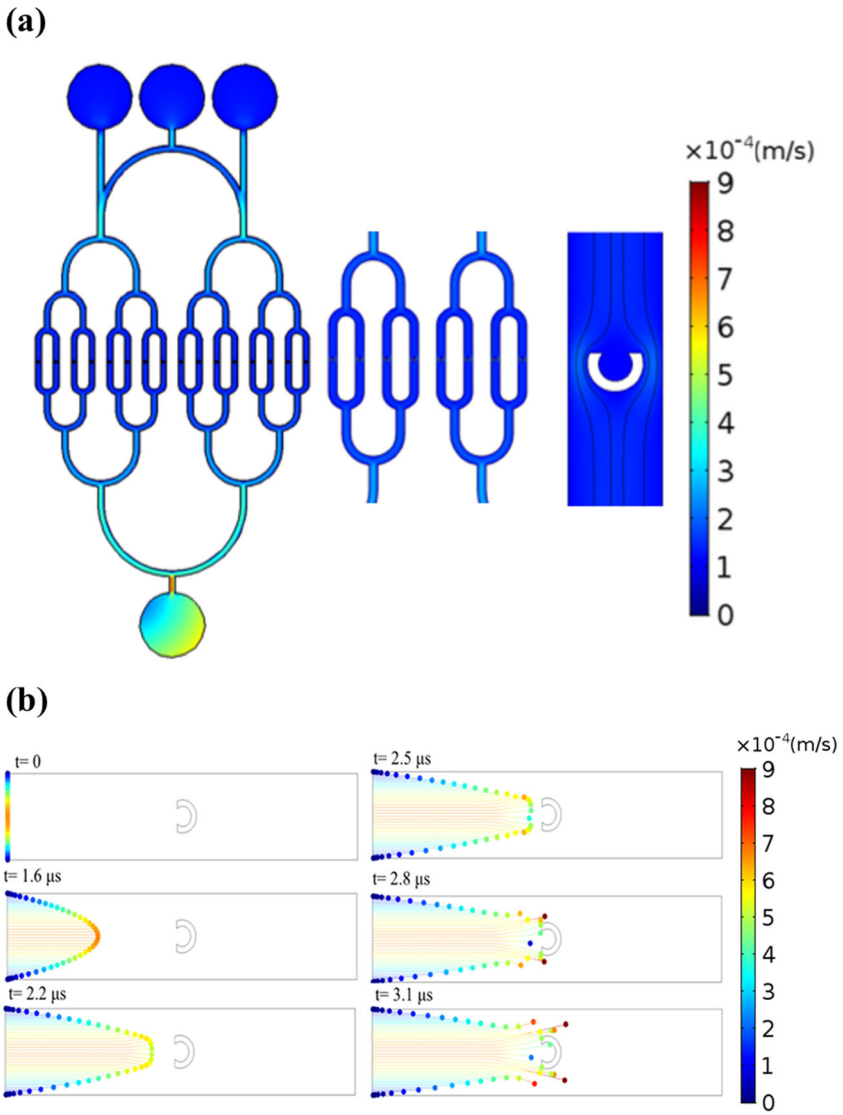


**Fig. 2** **a** Simulation of trapping mechanism with parallel channel designs showing 16 equivalent stagnation points in C shaped regions. **b** Particle tracing at different time points

by using Nikon Ti-E inverted fluorescent microscope, brightfield and fluorescence microscopy images (60X lens) were taken every 9 min and luminescence of Nop56:RFP was followed. A sequence of captured brightfield images of a trapped cell showing its budding process can be seen in Fig. 3 as an example. When cells were trapped inside the device, their morphological changes and cell cycle can be tracked. Variation in budding times and cell status before and after drug treatment can be observed. An example to taken fluorescence images and how they can be superimposed on top of brightfield images to follow Nop56:RFP concentration can be seen in Fig. 5.

## 3 Results and discussion

Cell cycle is the series of events happening in cell with the DNA duplication, organelles to produce two daughter cells and cytoplasm division. $G_1$, S, $G_2$ and M are the 4-phases of cell cycle (Fig. 4). Actively dividing eukaryotic cells undergo these phases and the cell grows and divides into two identical cells. In the $G_1$ phase, cell size increases and cellular components double. DNA replication (replication of chromosomes from 23 to 46) occurs in S phase. In the $G_2$ phase cells prepare themselves for cell division and in the M phase cytokinesis (cytoplasm division) takes place. At the end of this process

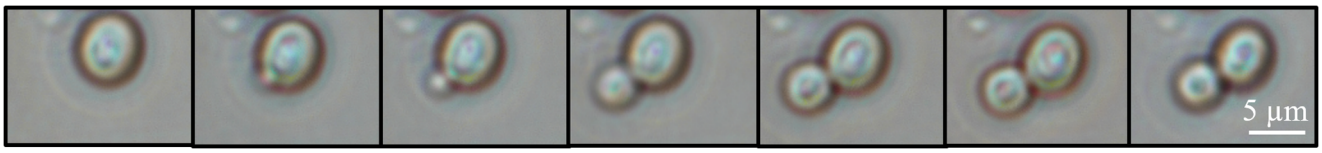


**Fig. 3** Microfluidic device used for single cell tracking

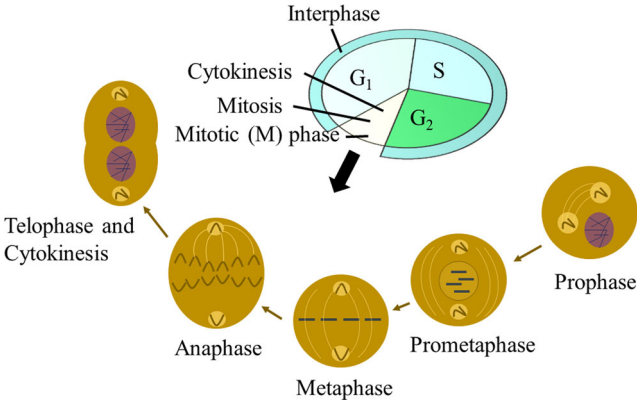


**Fig. 4** Schematic representation of cell cycle phases and checkpoints

two identical daughter cells form (Fang et al. 2019). In yeast, the cell division is affected by ribosome biogenesis, which starts at the nucleolus and is related to ribosome production. It is a complicated and tightly coordinated process (Bernstain et al. 2007; Lempiäinen and Shore 2009; Leary and Huang 2001; Gomez-Herreros et al. 2013; Ebersberger et al. 2014; Thomson et al. 2013). When cells pass through START mechanism in late G1 phase, cell division process begins (Polymenis and Aramayo 2015). The size of the cell at division and the ribosome numbers are related to the growth rate. Although up to date studies have implied various interactions between cell cycle and ribosome synthesis in cells (Bernstain et al. 2007; Dez and Tollervey 2004), there are still gaps of knowledge of that relationship. In order to observe the changes in ribosome assembly/pre-processing and cell cycle in response to the growth inhibitory drugs, RFP tagged Nop56 nucleolar protein is selected. Nop56 is an essential evolutionarily-conserved nucleolar protein, and is required for ribosome synthesis (Lafontaine and Tollervey 2000). Nop56 expression as well as the critical cell size for budding of yeast cells are followed in in-house fabricated dual purpose microfluidic bioreactor system. Hydroxyurea (HU) and metformin are chosen as the inhibitors of DNA and TOR pathway, respectively.

### 3.1 Effect of DNA synthesis inhibitor hydroxyurea on yeast cells

The changes in cell cycle as well as in protein synthesis within the yeast cells were followed under the application of the antitumor agent HU applied to the one side of the chip. In Fig. 5, the expression of RFP tagged nucleolar Nop56 gene product can be tracked in single live cells before, during and after HU treatment. Before HU application, each cell continued its normal life cycle. The cells' luminescence was significantly decreased during HU treatment period, as the DNA replication was inhibited by HU treatment (Fig. 5). When the HU feeding

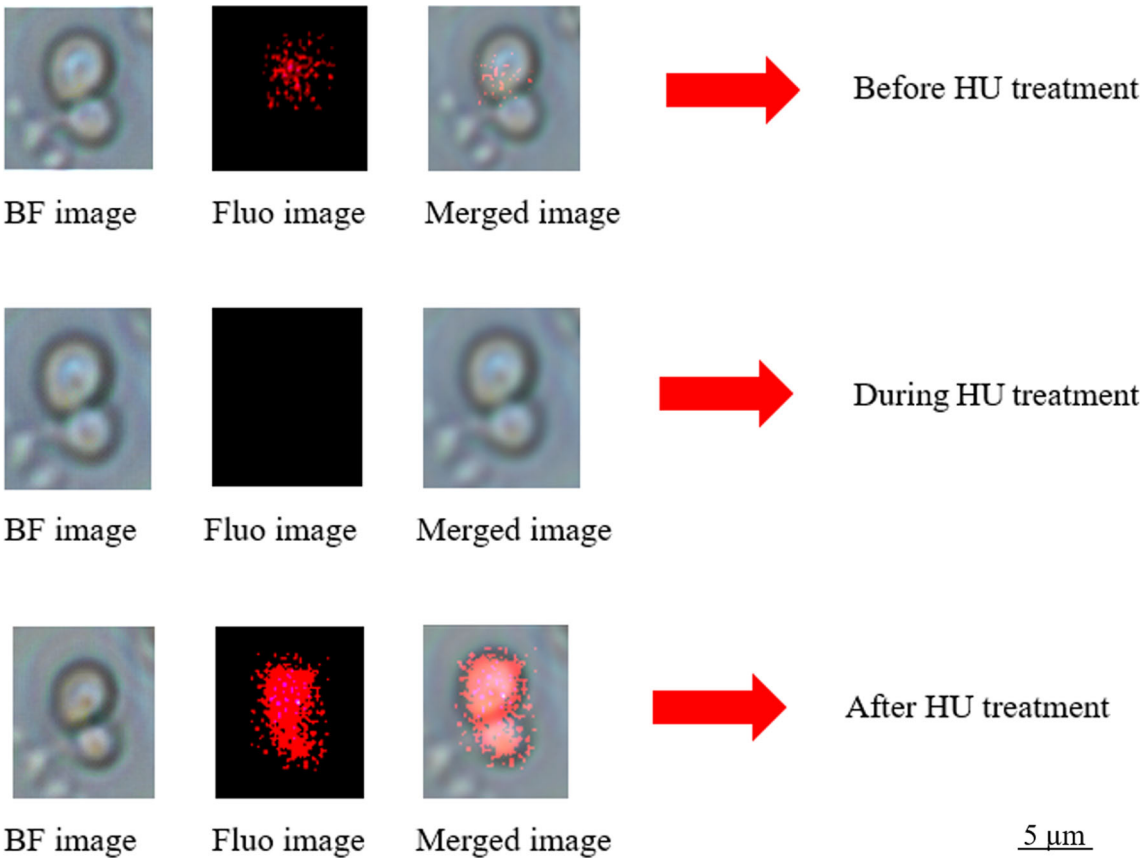


**Fig. 5** The brightfield (BF), fluorescence (Fluo) and merged microscopy images of yeast cells before, during and after hydroxyurea (HU) treatment

was stopped and fresh nutrient medium was flown through the microbioreactor, the cells recovered themselves slowly and luminescence increased.

Figure 6 a shows stable cell count in yeast population under steady state conditions including the HU treatment period. There was neither proliferation nor cell death in between the 435th and 610th minutes (Fig. 6a). After the HU treatment, cell count increased gradually (from 55 to 70 cells) towards the end of the experiment. When the total cell perimeter was considered as a representation of biomass synthesis rate, there was a decrease in dimensions of the cells during HU feeding period. However, after the HU treatment, the cells were able to recover, and increase in size was observed through the end of the experiment (Fig. 6b). The total fluorescence intensity of the cell population was decreasing in a certain time interval before the HU treatment period (Fig. 6c). That time might coincide with the mitosis phase (M phase) of the cells where the protein synthesis slows down. During HU treatment, the fluorescence intensity got closer to zero at some points, indicating suppression of Nop56 expression or inviability. The reason for this might be that, HU slows down the S-phase of the cell cycle and it suppresses the cell proliferation event. Consequently, the protein synthesis, which should follow Nop56 protein expression, did not take place within the cell. Since HU is a DNA synthesis/replication inhibitor, it affects the progression of S-phase. HU treatment causes S phase to continue in slow motion but does not cause to stop the cell cycle. Cells probably maintained their regular evolution, as increasing trend in the fluorescence intensity was observed after the release of HU through the end of the experiment, where protein synthesis seems to be the dominating process compared to proliferation. We may speculate that, after the release of HU, the cells are maintaining themselves and during this maintenance step Nop56 protein might have a role in DNA repairing. The role of nucleolar protein Nop56p in DNA replication has already been reported (Bogomolnaya et al. 2004). Nop56 is used before the initiation of DNA replication, shortening the duration of G1 phase of the cell cycle (Bogomolnaya et al. 2004). In our experiments, the duration of G1 phase took 26.5 min on average (Fig. 6d), and the cell cycle duration took 112 min before HU administration. However, after HU treatment, the cell cycle duration changed to 131 min. When the data at 900th minute were considered, all of the cells recovered themselves. This result proves that, although HU slows down the cell cycle mechanism, it does not kill the cells. As also observed by the time profile of

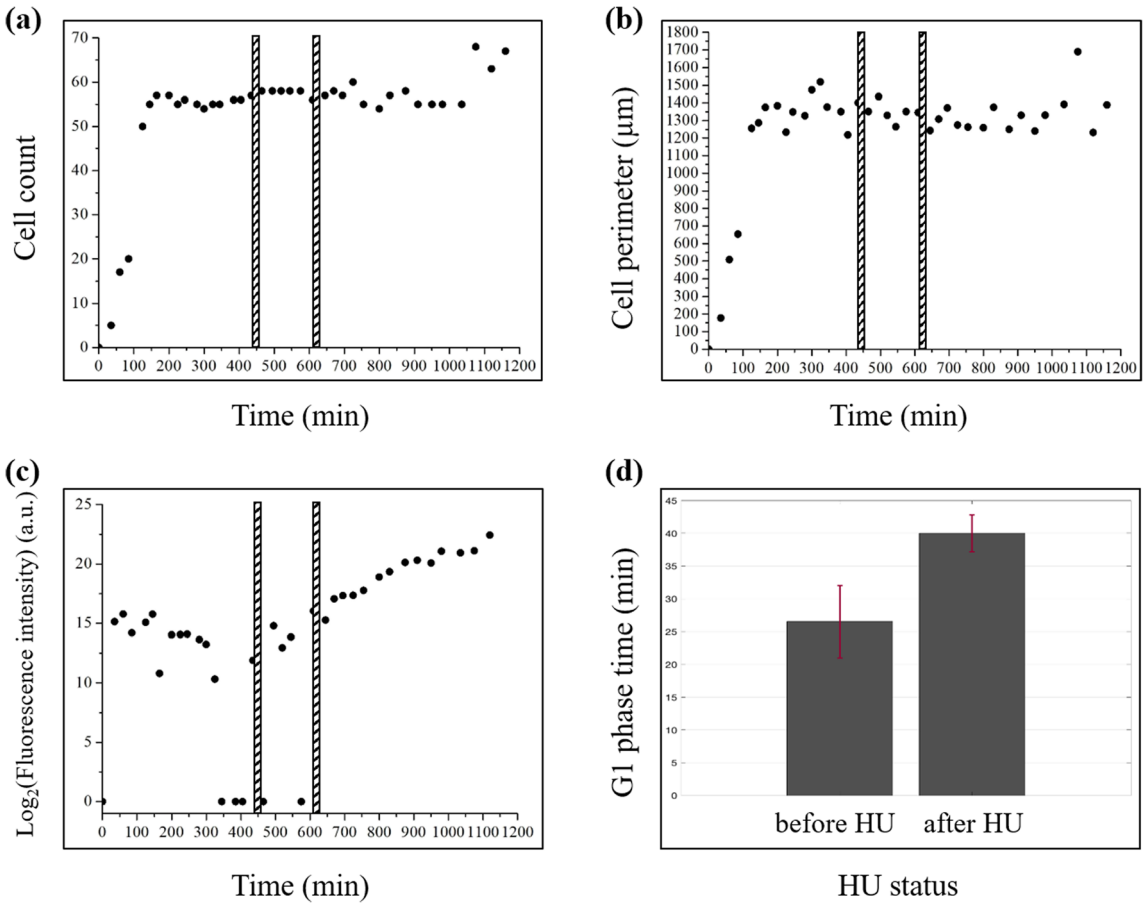


**Fig. 6** **a** Time profile of the cell count. **b** Time profile of the cell perimeter (population). **c** Time profile of the fluorescence intensity (Vertical lines indicate the start and end of HU application). **d** Duration of G1 phases before and after HU treatment

perimeter, the biomass synthesis rate is sustained after the cessation of HU application.

### 3.1.1 Single cell dynamics in HU experiment

The typical examples of single cells obtained in the experiments are discussed below in terms of the effects of HU inhibitor on cell cycle, cell dimension and Nop56 expression (protein synthesis). In the presence of HU, elongated ellipsoidal yeast cells were observed in YNB medium (Fig. 7a) and the Nop56 gene expression was repressed. HU might have suppressed ribosome biogenesis proteins and generated elongated cell morphology. Similarly, in literature, it was reported that the repression of most of the ribosome biogenesis proteins (20S and 60S proteins) caused an excessive extension in the buds of the yeast cells (Thapa et al. 2013). In YNB medium, if HU was not present in the medium, G1 phases of the single cells took 32 ± 11 min, in agreement with literature. The doubling times were around 112 and 131 min, before and after HU treatment (in fresh nutrient medium), respectively. In the presence of HU, for example, Cell 4 and Cell 9 started budding after 233 min of coming to the chamber, i.e.. G1 phase of these cells actually took more time than 233 min. Similarly, in literature reports, suppressing the synthesis of most 40S ribonucleoprotein subunit proteins led to the arrest of the cell cycle at G1 phase or dramatically slowed down the G1 phase (Thapa et al. 2013). It was highly probable that the yeast cells exposed to HU at high concentration had slightly higher critical volume to divide as shown in Fig. 7b.

The fluorescence intensity of some single cells fell to almost zero after HU application as shown in Fig. 7c. On the other hand, at the end of the experiment, the cells' integrated fluorescence density increased indicating cell viability and recovery. In order to complete the cell cycle, protein synthesis is necessary. We observed that the ribosomal protein Nop56 was extensively expressed when the single cell perimeter is around 14–16 μm. This can be seen in Fig. 7c, where fluorescence density is plotted versus cell perimeter. This corresponds to G1 phase of the cell cycle. Nop56 expression was significantly decreased when the live single cell's perimeter increased to more than 20 μm, i.e. at the end of cell cycle, probably the M phase. Cells require a rapid protein synthesis during $G_1$ to create crucial regulatory proteins. Moreover, protein synthesis is also needed to complete the $G_2$ phase and

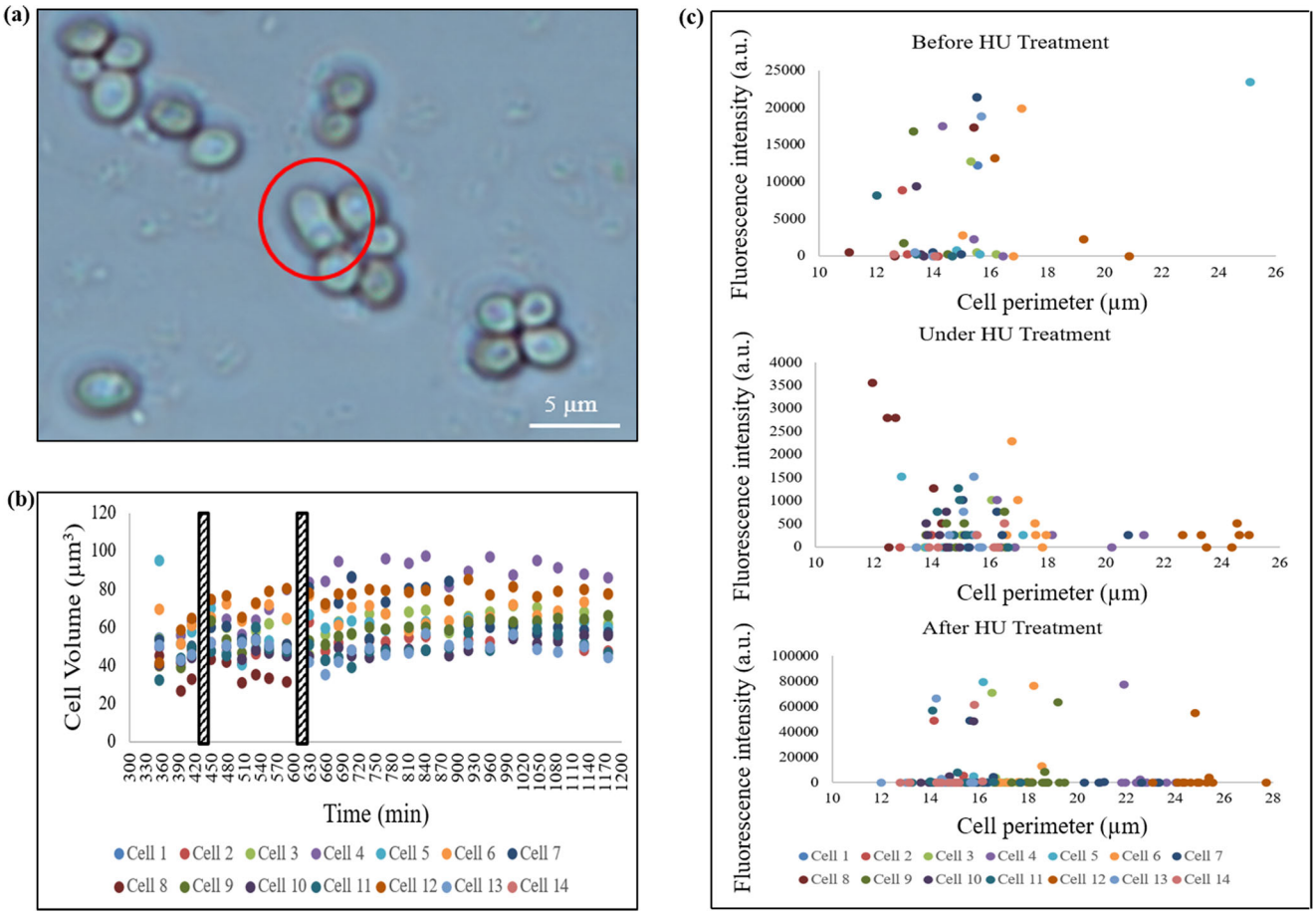


**Fig. 7** **a** Long spheroidal shape of yeast cell during YNB HU experiment (Chamber 2). **b** Time profile of single cell volume during YNB HU experiment (Chamber 1). **c** Time profiles of single mother and daughter cells integrated fluorescence density and perimeter before, during and after YNB HU experiment (Chamber 1)

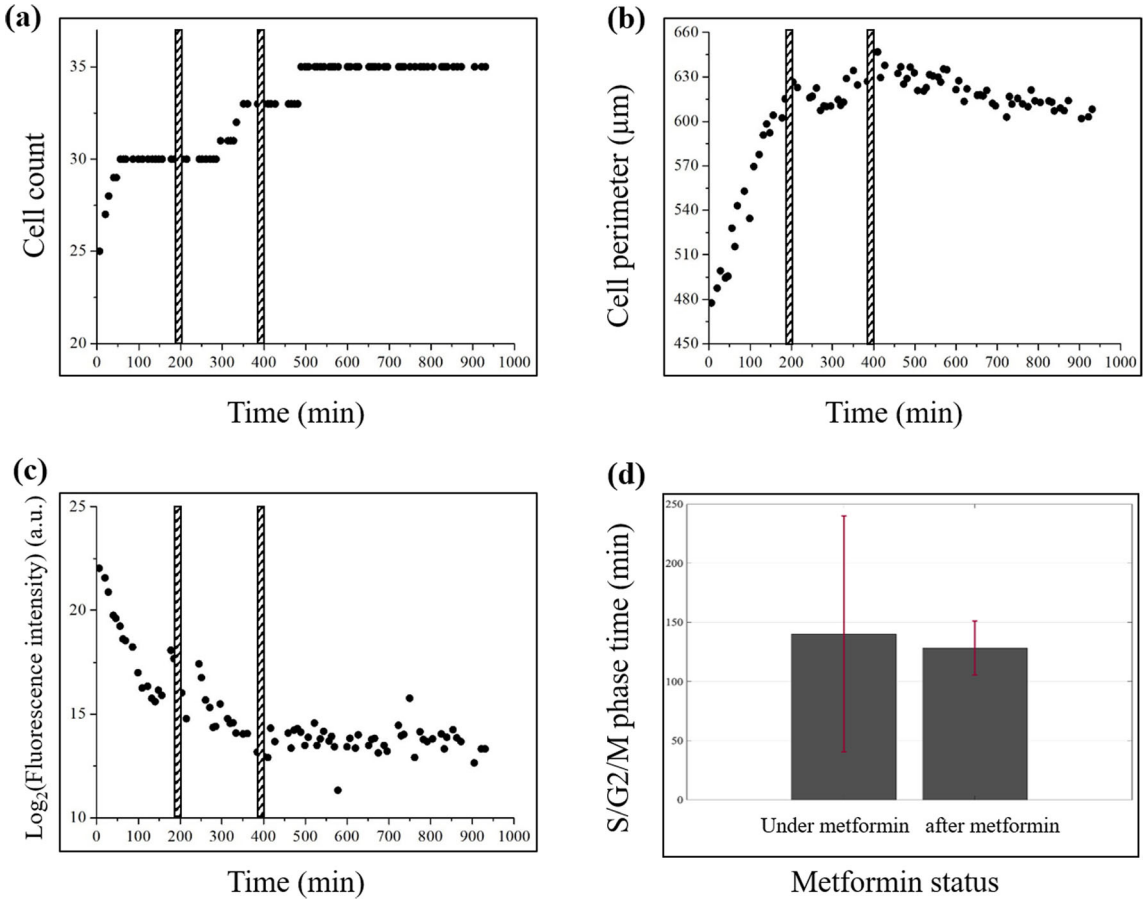


**Fig. 8** **a** Time profile of cell count. **b** Time profile of cell perimeter (population). **c** Time profile of the fluorescence intensity (Vertical lines indicate the start and end of metformin application). **d** Duration of S/G2/M phases before and after metformin treatment

enter mitosis (Burke and Church 1991). In budding yeast cells; a conserved transcriptional activation of ribosome biogenesis was reported before the cells started a new round of cell division, i.e. at G1 phase (Blank et al. 2017).

#### 3.1.2 Discussion on HU application

HU treatment causes inhibition of ribonucleotide reductase (RNR), inhibition of the ribonucleoside diphosphate reductase (Madaan et al. 2012) and subsequent deoxyribonucleoside triphosphates (dNTPs) production (Dubacq et al. 2006; Alvino et al. 2007; Koç et al. 2004). dNTPs appear when cells enter S phase and induce an S-phase checkpoint response, which results in transcriptional activation of RNR genes and prevention of cell-cycle progression (Dubacq et al. 2006). HU, thus, interferes with the S phase progression and engages the checkpoint to prevent the passage into a catastrophic mitosis throughout the cell cycle. Although, many studies stated that, HU does not affect protein synthesis (Alvino et al. 2007), it might have an effect on ribosome biogenesis (Kihlman et al. 1966; Johnston 1980; Scala et al. 2016). If ribosome biogenesis is hindered, an Rb-like protein (Whi5)-dependent mechanism restrains cell cycle commitment event (START) (Lempiäinen and Shore 2009). Thus, ribosome biogenesis and protein synthesis are the major steps of cell proliferation. Ribosomes direct the $G_1$-S phase transition, hence control the cell cycle progression.

### 3.2 Effect of mTOR inhibitor metformin on yeast cells

Cell growth comprising of transcription, translation, protein degradation etc. is regulated by the target of rapamycin (TOR) pathway. The proteins in the mammalian TOR family are conserved from yeast to man (Mayer and Grummt 2006). Transcription, protein synthesis, ribosome biogenesis, nutrient transport and mitochondrial metabolism are the anabolic processes governed by the TOR. On the other hand, mRNA degradation, ubiquitin-dependent proteolysis, autophagy and apoptosis are the negatively regulated catabolic processes by TOR (Hall 2008). Stalling of cell growth and release of autophagic processes are the results of the absence of mTORC1 signaling.

In this part of the work, the response of yeast cells to mTOR inhibitor, the drug metformin, was investigated to reveal the role of mTOR signaling in ribosome biogenesis/synthesis and cell proliferation on the other side of the chip

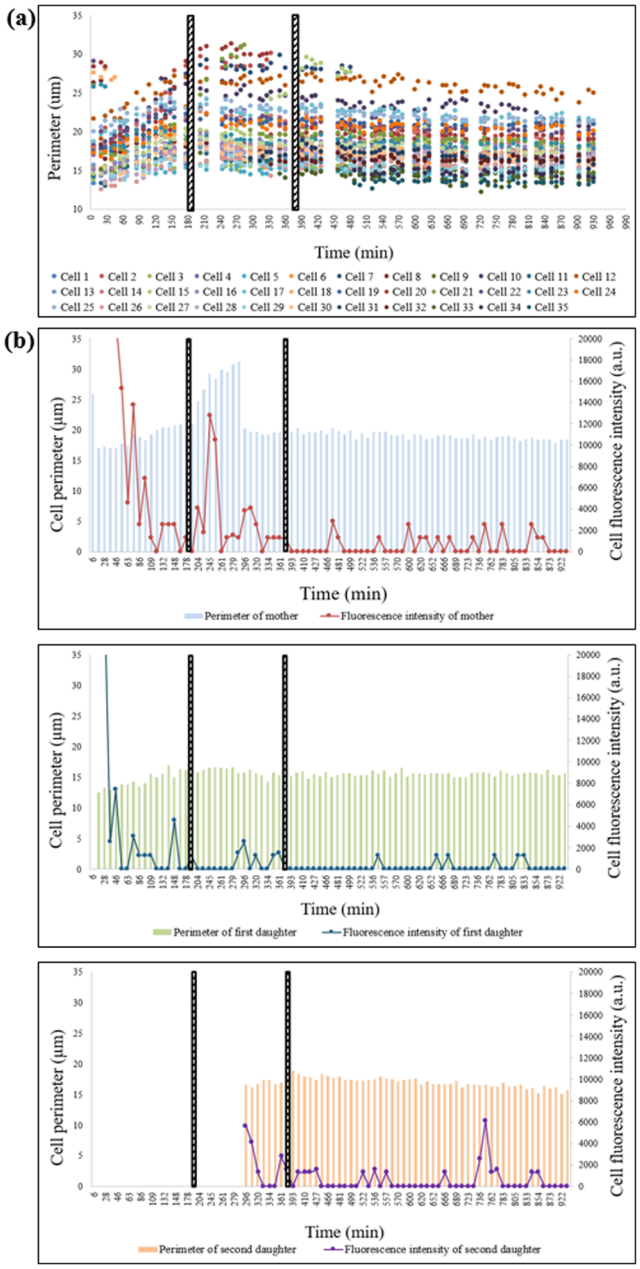


**Fig. 9** **a** Time profiles of the single cells. **b** Time profiles of single mother and daughter cells integrated fluorescence density and perimeter before, during and after metformin experiment

while the cells on the previously mentioned side of the chip were under the influence of the anti-tumor agent HU. Under the experimental conditions of metformin, the cell count increased in the first 500 min including the drug treatment period (Fig. 8a). Total cell perimeter also increased continuously until the drug application. However, it slightly decreased due to metformin effect on the cells, in spite of the increase in cell count during the metformin application period (Fig. 8b). Cell growth is identified as an increase in cell size rather than an increase in cell number which is the outcome of the cell division (Hall 2008). Since metformin acts as the cell growth inhibitor, a decrease in cell size is a reasonable outcome. Since metformin is used to regulate the insulin level, the glucose uptake mechanism of cells might be disturbed. Cells continued to cell division, so cell count increased, but their dimensional growth (cell size) decreased due to metformin effect on cells.

The Nop56 protein expression of the total cells (population) is displayed in Fig. 8c. In the first 100 min, the fluorescence intensity of the cells was very high but decreasing. During the metformin application period, this decreasing trend of the fluorescence intensity continued. There is an increase in the intensity concomitant with the decrease in cell size at the 250th min. However, as the drug supply continued, a decrease in the fluorescence intensity was seen, followed by its stabilization. This result is in agreement with the reports on another mTOR inhibitor, rapamycin, which inhibited the gene expression of r-proteins (Kakihara et al. 2014; Sinclair 2005). Moreover, there is an extension in the time of S/$G_2$/M phase due to metformin application (Fig. 8d).

In order to capture cell to cell variations, each cell was individually analyzed in the metformin treatment experiment. The perimeter change of every cell at the given time intervals (before, during and after metformin exposure) can be seen in Fig. 9a. Although the perimeters of many single cells were decreasing towards the end of the experiment, these cells continued their proliferation during and after the drug application. The dimension of the first daughter increased before the drug application, but a decreasing trend can be seen during the drug treatment period (Fig. 9b). During metformin application, Nop56 expression in mother cell increased in parallel to the increase in single cell perimeter, i.e. highest during the S/G2/M phase of cell cycle (Fig. 9b), but decreased significantly towards the end of the cell cycle, most probably during mitosis phase. The daughter cells had comparable levels of Nop56 expression with their mother. Under normal conditions, yeast cells complete their cell cycle at around 80–110 min. However, under metformin treatment, it took 220 min to have the daughter cell. i.e., metformin caused the prolongation of the cell cycle. Moreover, if the daughter cell were born after the metformin application, it could never bud again.

### 3.2.1 Discussion on metformin

TOR pathway is necessary for RNA transcription, and it takes part in the regulation of RNA polymerase I and II. The gene expressions related to r-proteins were reported to be inhibited by mTOR inhibitor rapamycin (Powers and Walter 1999). TOR signaling pathway was deactivated by rapamycin and yeast cells behaved like at starvation conditions, and the core proteins of C/D box were transferred from the nucleolus to nucleoplasm (Kakihara et al. 2014). Rapamycin also induced sporulation of diploid yeast cells under suitable conditions (Powers and Walter 1999). Our findings obtained in this

0.14 nL volume microfluidic bioreactor are in agreement with these literature results, which were obtained in shake flasks or macroscale systems.

In the last decade, the relation between metformin and cancer is also examined, where metformin treatment of type2 diabetes (T2D) patients led to a decreased risk of cancer (Kasznicki et al. 2014). High levels of circulating insulin/IGF1 and upregulation of insulin/IGF receptor signaling pathways participate in the generation of cancer cells. Thus, metformin is used to adjust the insulin level, inactivate insulin/IGF signaling pathways and adapt cellular survival (Kasznicki et al. 2014). Insulin/IGF-1 is responsible for the adjustment of glucose uptake and carcinogenesis via upregulation of insulin/IGF receptor signaling pathway. Excess amount of food consumption results in increased production of IGF-1, which binds to IGF-1 receptor and insulin receptor. Subsequently, insulin receptor substrate (IRS) transmits the signal to phosphoinositide 3-kinase (PI3K) and Akt/protein kinase B (PKB), which triggers mTORC1. So this pathway need to be suppressed in order to cope with T2D and consequent cancer. The emergence of mTOR inhibitors as anticancer agents has been largely preceded by rapamycin analogs (Zheng and Jiang 2015). Currently these analogs include temsirolimus, everolimus, ridaforolimus and deforolimustan. mTOR inhibitors have been highlighted for their safety and efficacy in cancer patients.

## 4 Conclusion

Microfluidic systems continue to be applied to cell biology. They try to show behavior of individual cells, confirm existing chemical and biological pathways or unveil new ones. Similarly in this work, we used COP based microfluidic bioreactor to perform cell biology experiments successfully. It provided several advantages such as; real time observation of the yeast cells, suitability for single cell studies, conduction of two different experiments at the same time under equal conditions and being durable to long-lasting experiments. The brightfield and fluorescence (tracking RFP:Nop56) microscopy images of the yeast cells trapped into the C-shaped regions were successfully recorded during the experiments. DNA inhibitor HU and mTOR inhibitor metformin were used for the first time in a microfluidic study, and their effects on the single yeast cells were investigated under continuous flow. The results obtained in this microfluidic system are in agreement with those at macroscale: While HU inhibited DNA replication due to the disturbance of S-phase, metformin slowed down cell growth. Moreover, in the present study, the expression of the nucleolar protein Nop56 of ribosome assembly and synthesis was densely observed during G1 phase of cell cycle, where the single cell perimeter representing the biomass synthesis rate was around 15 μm, and later towards the end of cell cycle, probably during M phase, the ribosomal protein expression slowed down. Under metformin treatment, the perimeters of single cells were observed to decrease, implying a decrease in biomass growth; however these cells continued their proliferation during and after the drug application. Moreover, Nop56 expression was observed both in G1 phase as well as in S/G2/M phases. Thus, these findings indicate that metformin extends the lifespan of the cells as expected despite the dimensional changes.

The relation between ribosome biogenesis and cell cycle was successfully investigated on single cell basis, capturing cell-to-cell variations, which cannot be tracked at regular macroscale bioreactors. As the heterogeneity of cell populations is an important issue in tumor cells, the present microfluidic platform can effectively be used for studying the drug effects on tumors and may shed light on the putative treatment strategies towards cancer.

**Acknowledgements** This work was supported by Bogazici University Research Fund through projects 13641D and 14261R.

## Compliance with ethical standards

**Conflict of interest** There are no conflicts to declare.

## References

G.M. Alvino, D. Collingwood, J.M. Murphy, J. Delrow, B.J. Brewer, M.K. Raghuraman, Mol. Cell. Biol. **27**, 6396 (2007)
M.C. Bélanger, Y. Marois, J. Biomed. Mater. Res. **58**, 467 (2001)
K.A. Bernstain, F. Bleichert, J.M. Bean, F.R. Cross, S.J. Baserga, Mol. Biol. Cell **18**, 953 (2007)
H.M. Blank, R. Perez, C. He, N. Maitra, R. Metz, J. Hill, Y. Lin, C.D. Johnson, V.A. Bankaitis, B.K. Kennedy, R. Aramayo, M. Polymenis, EMBO J. **36**, 487 (2017)
L.M. Bogomolnaya, R. Pathak, R. Cham, J. Guo, Y.V. Surovtseva, L. Jaeckel, M. Polymenis, Curr. Genet. **45**, 350 (2004)
D.J. Burke, D. Church, Mol. Cell. Biol. **11**, 3691 (1991)
C. Dez, D. Tollervey, Curr. Opin. Microbiol. **7**, 631 (2004)
C. Dubacq, A. Chevalier, R. Courbeyrette, C. Petat, X. Gidrol, C. Mann, Mol. Gen. Genomics. **275**, 114 (2006)
C. Dusny, A. Grünberger, Curr. Opin. Biotechnol. **63**, 26 (2020)
I. Ebersberger, S. Simm, M.S. Leisegang, P. Schmitzberger, O. Mirus, V. Von Haeseler, M.T. Bohnsack, E. Schleiff, Nucleic Acids Res. **42**, 1509 (2014)
D. Falconnet, R.J. Niemistö, M. Taylor, T.G. Ricicova, T. Galitski, I. Schmulevic, C.L. Hansen, Lab Chip **11**, 466 (2011)
H.S. Fang, M.F. Lang, J. Sun, Chinese J. Anal. Chem. **47**, 1293 (2019)
E. Gencturk, S. Mutlu, K.O. Ulgen, Biomicrofluidics **11** (2017)
Y.D. Gokdel, S. Mutlu, A.D. Yalcinkaya, J. Micromechanics Microengineering **20** (2010)
F. Gomez-Herreros, O. Rodriguez-Galan, M. Morillo-Huesca, D. Maya, M. Arista-Romero, J. de la Cruz, S. Chavez, M.C. Munoz-Centeno, J. Biol. Chem. **288**, 31689 (2013)
N. Haandbæk, S.C. Bürgel, F. Rudolf, F. Heer, A. Hierlemann, ACS Sensors **1**, 1020 (2016)
M.N. Hall, Transplant. Proc. **40**, 5 (2008)

A.S. Hansen, N. Hao, E.K. OShea, Nat. Protoc. **10**, 1181 (2015)
M.C. Jo, L. Qin, Small. **12**, 5787 (2016)
L.H. Johnston, Curr. Genet. **2**, 175 (1980)
Y. Kakihara, T. Makhnevych, L. Zhao, W. Tang, W.A. Houry, Genome Biol. **15**, 404 (2014)
J. Kasznicki, A. Sliwinska, J. Drzewoski, Ann. Transl. Med. **2**, 57 (2014)
B.A. Kihlman, T. Eriksson, G. Odmark, Here **55**, 386 (1966)
A. Koç, L.J. Wheeler, C.K. Mathews, G.F. Merrill, J. Biol. Chem. **279**, 223 (2004)
M. La Ferla, A. Mercatanti, G. Rocchi, S. Lodovichi, T. Cervelli, L. Pignata, M.A. Caligo, A. Galli, Mutat. Res. - Fundam. Mol. Mech. Mutagen. **774**, 14 (2015)
D.L.J. Lafontaine, D. Tollervey, Mol. Cell. Biol. **20**, 2650 (2000)
D.J. Leary, S. Huang, FEBS Lett. **509**, 145 (2001)
H. Lempiäinen, D. Shore, Curr. Opin. Cell Biol. **21**, 855 (2009)
K. Madaan, D. Kaushik, T. Verma, Expert. Rev. Anticancer. Ther. **12**, 19 (2012)
Z.S. Marinkovic, C. Vulin, M. Acman, X. Song, J.M. Di Meglio, A.B. Lindner, P. Hersen, Elife **8**, 1 (2019)
C. Mayer, I. Grummt, Oncogene **25**, 6384 (2006)
I. E. Odabasi, E. Gencturk, S. Puza, S. Mutlu, and K. O. Ulgen, 1 (2018)
A. Piruska, I. Nikcevic, S.H. Lee, C. Ahn, W.R. Heineman, P.A. Limbach, C.J. Seliskar, Lab Chip. **5**, 1348 (2005)
M. Polymenis, R. Aramayo, Microb. Cell **2**, 94 (2015)
T. Powers, P. Walter, Mol. Biol. Cell **10**, 987 (1999)
S. Puza, E. Gencturk, I.E. Odabasi, E. Iseri, S. Mutlu, K.O. Ulgen, Biomed. Microdevices **19**, 40 (2017)
F. Scala, E. Brighenti, M. Govoni, E. Imbrogno, F. Fornari, D. Treré, L. Montanaro, M. Derenzini, Oncogene **35**, 977 (2016)
G.W. Schmidt, O. Frey, F. Rudolf, Methods Mol. Biol. **1672**, 537 (2018)
F. Sherman, Encycl. Mol. Biol. Mol. Medinicine **6**, 302 (1997)
D.A. Sinclair, Mech. Ageing Dev. **126**, 987 (2005)
M. Thapa, A. Bommakanti, M. Shamsuzzaman, B. Gregory, L. Samsel, J.M. Zengel, L. Lindahl, Mol. Biol. Cell **24**, 3620 (2013)
E. Thomson, S. Ferreira-Cerca, E. Hurt, J. Cell Sci. **126**, 4815 (2013)
M.W. Toepke, D.J. Beebe, Lab Chip **6**, 1484 (2006)
T. Trantidou, Y. Elani, E. Parsons, O. Ces, Microsystems Nanoeng. **3**, 16091 (2017)
J.L. Woolford, S.J. Baserga, Genetics **195**, 643 (2013)
B.Y. Yu, C. Elbuken, C. Shen, J.P. Huissoon, C.L. Ren, Sci. Rep. **8**, 1 (2018)
X. Zhao, C. Luo, H. Wang, Integr. Biol. **11**, 79 (2019)
Y. Zheng, Y. Jiang, Mol. Cell. Pharmacol. **7**, 15 (2015)